Journal of Materials Science: Materials in Electronics
https://doi.org/10.1007/s10854-018-9329-0

Protein-derived nitrogen-doped hierarchically porous carbon as electrode material for supercapacitors

Peng Song[1] · Xiaoping Shen[1] · Wenfeng He[1] · Lirong Kong[1] · Xiaome He[1] · Zhenyuan Ji[1] · Aihua Yuan[2] · Guoxing Zhu[1] · Na Li[1]

Received: 6 April 2018 / Accepted: 17 May 2018

Abstract
This study aimed at developing supercapacitor electrode materials from textile industry waste, thereby mediating waste disposal problem through reuse. Through a simple two-step process, nitrogen-doped hierarchically porous carbons (NHPC) derived from sericin, a waste protein, were synthesized and used for electrochemical capacitors for the first time. The as-prepared NHPC with a specific surface area of 2723 $m^2\ g^{-1}$ and a pore volume of 1.42 $cm^3\ g^{-1}$ exhibited a high specific capacitance of 287 F g^{-1} at the current density of 0.5 A g^{-1}, which was comparable or even higher than that of numerous porous carbon materials reported previously. With this electrode, about 93% of the initial capacitance (221 F g^{-1}/5 A g^{-1}) was retained after 10,000 cycles, demonstrating a good cyclic stability. Moreover, the specific capacitance of sericin-derived NHPC is also better than that of fibroin-derived porous carbon. This work not only developed an effective way to prepare high-performance supercapacitor electrode materials from the waste protein, but also provided a strategy for its disposal issue and contributed to the environmental improvement.

1 Introduction

Supercapacitors, with combined advantages of conventional rechargeable batteries and capacitors, have attracted much attention in recent years [1–3]. These advantages, such as great power density and long cycle life, make it very promising in portable electronics, hybrid electric vehicles, and back-up power storage devices fields [4–6]. According to the energy storage mechanism, supercapacitors are divided into electrical double layer capacitors and pseudocapacitors [7]. In terms of the electrical double layer capacitors, carbon materials are the most commonly used electrode materials [8].

To date, various carbon materials, such as carbon nanotube [9], graphene [10], and carbon quantum dot [11], have been extensively studied as electrode materials for supercapacitors. Recent studies illustrated that doping with nitrogen could remarkably improve the electrochemical performance of carbon materials as nitrogen offered reversible pseudocapacitance effects [12, 13]. Unfortunately, the incorporation of nitrogen into carbon materials is often time-consuming, complicated, and costly [14]. By contrast, utilizing abundant and innoxius nitrogen-containing biomass to prepare nitrogen-doped carbon materials appears low-cost and very promising for commercial production [15–19].

Sericin, one of the two major proteins forming the cocoons [20, 21], is known as a waste material in the textile industry [22]. It is estimated that approximately 50,000 tons of sericin is abandoned annually worldwide, which has caused serious problems for water resources [23]. Undoubtedly, formulating an effective strategy focusing on the disposal issue of sericin is highly desired. In fact, sericin, as a natural protein, is rich in carbon and nitrogen elements. This feature makes it a very promising precursor to prepare nitrogen-doped carbon materials for supercapacitors. However, to the best of our knowledge, the study on this topic has not yet been reported.

Electronic supplementary material The online version of this article (https://doi.org/10.1007/s10854-018-9329-0) contains supplementary material, which is available to authorized users.

✉ Xiaoping Shen
xiaopingshen@163.com

[1] School of Material Science & Engineering, School of Chemistry & Chemical Engineering, Jiangsu University, Zhenjang 212013, People's Republic of China

[2] School of Environmental & Chemical Engineering, Jiangsu University of Science and Technology, Zhenjiang 212003, People's Republic of China

Published online: 22 May 2018

Herein, we report a simple and effective way to develop novel nitrogen-doped hierarchically porous carbon materials (NHPC) using sericin as the raw material. The sericin-derived NHPC was produced through a two-step pre-carbonization and KOH activation process. The electrochemical performances of NHPC as supercapacitor electrode were investigated. As far as we know, this is the first research to evaluate the possible application of sericin in the electrochemical energy storage field.

2 Experimental

2.1 Materials

The *Bombyx mori* silkworm cocoons were provided by the Sericultural Research Institute, Chinese Academy of Agricultural Sciences (Jiangsu, China). Hydrochloric acid (HCl), potassium hydroxide (KOH), and *N*-methyl-2-pyrrolidone (NMP) were bought from Sinopharm Chemical Regent Co. Ltd (Shanghai, China). Polyvinylidene fluoride (PVDF) was purchased from Aladdin Chemistry Co., Ltd. (Shanghai, China). All reagents are of analytical-grade, and used as received without further purification.

2.2 Sericin extraction

Sericin was extracted from cocoons using a chemical-free method [24]. In brief, cocoon pieces were mixed with distilled water in a mass ratio of 1:25 (4 g of silk cocoon: 100 g of water). The mixture was autoclaved at 120 °C for 1 h, and then filtered with a nonwoven filter paper. After that, the sericin solution was frozen overnight at − 20 °C, and finally lyophilized at − 50 °C for 48 h.

2.3 Preparation of sericin-derived NHPC

The sericin-derived NHPC was prepared through a two-step pre-carbonization and KOH activation process. The schematic diagram was shown (Fig. 1). In a typical synthesis, sericin was first pyrolyzed (pre-carbonized) at 400 °C for 2 h. The obtained material was mixed with KOH, and then further pyrolyzed in the tube furnace at 800 °C for another 2 h. The heating rate of 5 °C/min and Ar atmosphere were applied for the both carbonization processes. Three different NHPC samples of $NHPC_1$, $NHPC_2$ and $NHPC_3$ were produced by using different mass ratios of KOH to pre-carbonized sericin powder of 1:1, 2:1 and 3:1, respectively. The solid products were grinded to powder, washed with 10% HCl, and thoroughly washed with distilled water. Finally, the products were dried at 100 °C.

2.4 Characterizations

X-ray diffractometer (XRD, D8 Advance, Bruker, Germany) with Cu K_α radiation operated at 40 kV and 40 mA was used to test the phase structure of NHPC. Raman spectrum was measured at room temperature using a DXR Raman spectrometer (Thermo Fisher Scientific, USA). The morphology and microstructure of NHPC were determined by scanning electron microscopy (SEM, S-4800, Hitachi, Japan) and transmission electron microscopy (TEM, Tecnai G2 F30 S-TWIN, FEI, USA). Brunauer–Emmett–Teller (BET) specific surface area and pore size distribution of NHPC were studied by a Micromeritic TriStar II 3020 analyzer (Micromeritics, USA). Element determinations were performed on a Flash1112A elemental analyzer (Thermo Fisher Scientific, USA). Surface chemistry was analyzed by X-ray photoelectron spectroscopy (XPS) using a RBD upgraded PHI-5000C ESCA system (Perkin Elmer, USA). XPS spectra were calibrated by the C 1 s signal at 284.6 eV.

2.5 Electrochemical measurements

Three-electrode configuration was used to evaluate the capacitive performance of NHPC on CHI 760E electrochemical workstation (Shanghai ChenHua Instruments Co., China). Hg/Hg_2Cl_2 (Saturated KCl) and platinum foil were used as the reference and counter electrodes, respectively. The working electrode was prepared by mixing activated materials (NHPC), acetylene black, and polyvinylidene fluoride (PVDF) with a mass ratio of 8:1:1 onto a nickel foam substrate (1 cm × 1 cm),

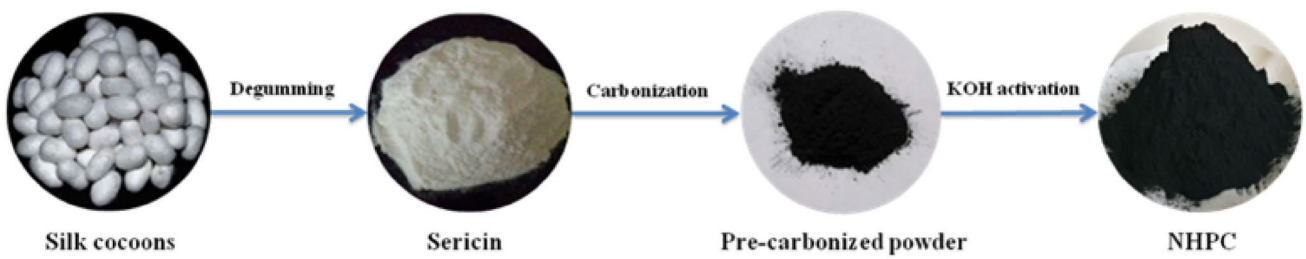

Fig. 1 Schematic illustration of the preparation process of NHPC

followed by pressing under a pressure of 10 MPa. After that, the electrode was dried at 80 °C overnight in a vacuum. The mass loading of NHPC on the working electrode was about 2 mg. The electrochemical characteristics of NHPC were studied by cyclic voltammetry (CV), galvanostatic charge–discharge (GCD), and electrochemical impedance spectroscopy (EIS) in 6.0 M KOH solution. The CV scans were measured in a potential window from − 1.0 to 0 V (vs. Hg/Hg_2Cl_2). The EIS measurement was studied in the frequency range of 100 kHz–10 mHz at open circuit potential with an ac perturbation of 10 mV. The specific capacitances of NHPC were determined via GCD measurements. All electrochemical studies were tested at room temperature.

A symmetric supercapacitor was fabricated by two NHPC-based electrodes with same mass loading (about 2 mg) and a porous cellulose membrane, and 6.0 M KOH was used as the electrolyte solution. The specific capacitance of single electrode is determined with equation of $C = 4It/(mV)$, in which C is the capacitance of the single electrode; I, t, V, and m stands for the discharge current (A), the discharging time (s), the potential change within the discharging time (V), and the total mass loading of active materials in both electrodes (g). The energy density (E) and power density (P) of the symmetric supercapacitor system are defined by equation of $E = CV^2/28.8$ and $P = 3600\ E/t$, where V is the voltage range, and t is the discharge time.

3 Results and discussion

3.1 Synthesis and characterization

Specific surface area, porous structure and pore size distribution were of great significance for the electrochemical performance of carbon materials [19]. During the past decades, various reagents, such as $ZnCl_2$, H_3PO_4, KOH, K_2CO_3, have been used to activate the raw carbon materials. In this work, KOH was selected as the activator because of its lower activation temperature and higher yield. Although the transformation of nitrogen species during the activation process has not been well understood, the activation mechanism for the resulting NHPC products might be explained as follows [25]:

$$6KOH + 2C \rightarrow 2K + 3H_2 + 2K_2CO_3;$$

$$K_2CO_3 \rightarrow K_2O + CO_2;$$

$$CO_2 + C \rightarrow 2CO;$$

$$K_2CO_3 + 2C \rightarrow 2K + 3CO;$$

$$K_2O + C \rightarrow 2K + CO.$$

SEM and TEM tests were carried out to study the microstructure of NHPC (Fig. 2). For comparison, the other carbon material produced by direct carbonization without KOH activation was also studied (Fig. S1). It is clear that the non-activated carbon material has a very dense surface (Fig. S1), while a well-developed porous structure is exhibited for NHPC with the help of KOH activation process (Fig. 2a, b). TEM images also reveal a porous structure for NHPC, as shown in Fig. 2c, d. From the images, a large amount of nano-scale pores are observed on NHPC. These pores could provide many convenient paths for transportation and penetration of electrolyte ions, which are of great importance for the fast ion transfer [18]. On the other hand, according to the Fig. 2, the pore size of NHPC is estimated ranging from a few nanometers to several micrometers. This phenomenon is consistent with the corresponding results reported in other literatures [26–28].

To further clarify the pore structure of NHPC, the samples ($NHPC_1$, $NHPC_2$, and $NHPC_3$) were examined by nitrogen adsorption–desorption isotherms. The results are shown in Fig. 3, and the corresponding parameters are summarized in Table 1. As shown, the BET specific surface areas of these samples are all higher than 1200 $m^2\ g^{-1}$, demonstrating a good activation effect caused by KOH. Specifically, $NHPC_2$ possesses a large BET specific surface area of 2723 $m^2\ g^{-1}$, which is 29 and 114% higher than that of $NHPC_1$ and $NHPC_3$, respectively. This result indicates that the used amount of KOH (activator) has a remarkable effect on the specific surface area of the resulting porous carbon materials, which is in good agreement with other studies [29–33].

According to the pore size distribution from BJH method, these NHPC samples possess a mixed microporosity (< 2 nm) and mesoporosity (2 ~ 50 nm) structure, as shown in Fig. 3b. The average pore sizes of NHPC are calculated to be about 2.2 nm (Table 1). It is evident that the specific surface area and pore volume increase as the mass ratios of KOH to the pre-carbonized sericin powder increases from 1 to 2. As the ratio rises to 3, although the average pore size and pore size distribution of the sample are almost unchanged, the specific surface area and pore volume are distinctly reduced, which are possibly owing to the collapse of the pores [34]. Actually, through SEM and TEM tests, macroporosity (> 50 nm) was also found on NHPC (Fig. S2). It confirms that the as-prepared NHPC is a combination of microporosity, mesoporosity and macroporosity, resulting in a hierarchically porous structure. This structural feature likely leads to a better electrochemical performance. Noticeably, compared with $NHPC_1$ and $NHPC_3$, $NHPC_2$ exhibits a much higher specific surface area and a similar pore size distribution. As a result, further study was mainly focused on $NHPC_2$.

XRD pattern of $NHPC_2$ displays two diffraction peaks, as shown in Fig. 4a. The broad peak located at $2\theta = 23.3°$ corresponds to the (002) diffraction, and the weak peak at $2\theta = 43.8°$ is attributed to the (100) diffraction. Both of them represent graphitic carbon with some disorder

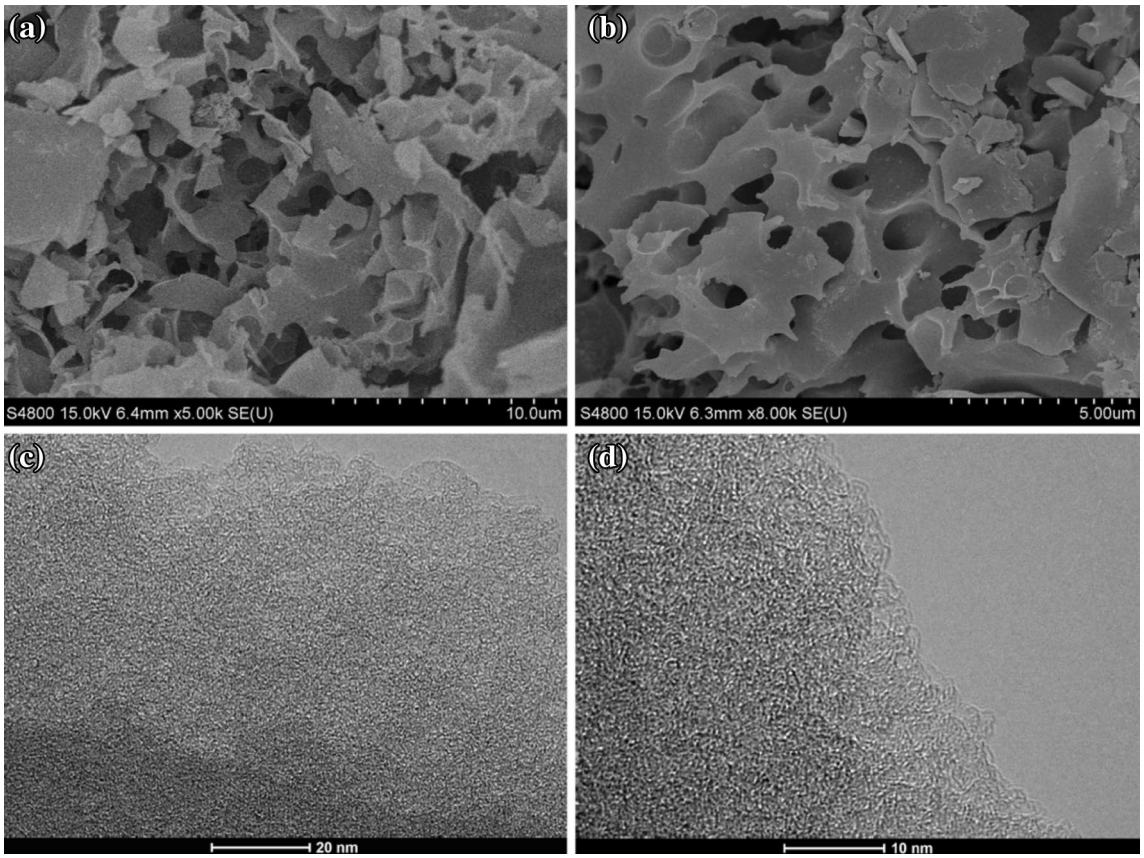

Fig. 2 **a, b** Typical SEM images and **c, d** TEM images of NHPC

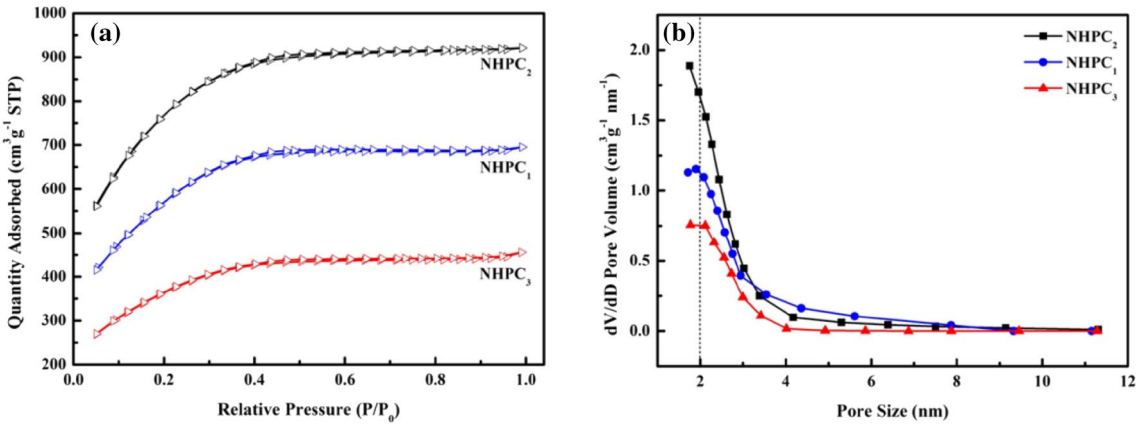

Fig. 3 **a** Nitrogen adsorption/desorption isotherms, and **b** corresponding pore size distribution curves of NHPC

structures [25, 35–37]. Furthermore, $NHPC_2$ was studied by Raman spectroscopy (Fig. 4b). As expected, two typical peaks located at around 1353 cm^{-1} (D-band) and 1590 cm^{-1} (G-band) are observed. The D-band is due to the breathing mode of *k*-point phonons of A_{1g} symmetry for the disordered graphite structure, while the G-band results from the E_{2g} phonon of sp^2-hybridized carbon atoms [38, 39]. It is known that the relative intensity of D-band to G-band (I_D/I_G) indicates the degree of structural disorder with respect to a perfect graphitic structure [40, 41]. Herein, the I_D/I_G value of $NHPC_2$ is determined to be 1.15, confirming the presence of disorder structure in

Table 1 Textural and structural characteristics of the NHPC

Sample	S_{BET}[a] ($m^2\ g^{-1}$)	V_t[b] ($cm^3\ g^{-1}$)	V_{micro}[c] ($cm^3\ g^{-1}$)	Average pore diameter (nm)
$NHPC_1$	2015	1.07	0.03	2.24
$NHPC_2$	2723	1.42	0.08	2.25
$NHPC_3$	1271	0.70	0.05	2.28

[a]BET surface area

[b]Total pore volume

[c]Micropore volume (d < 2 nm), obtained from the BJH distribution

the carbon matrix, which is in good accordance with the XRD result.

The nitrogen chemical state and nitrogen content of the resulting nitrogen-doped porous carbon materials are markedly influenced by activation process [42]. In order to evaluate the nitrogen doping degree and nitrogen bonding configuration in $NHPC_2$, XPS and elemental analyses were carried out (Fig. 5; Table 2). The results reveal the presence of carbon, nitrogen and oxygen in the product. The nitrogen content evaluated from the elemental analysis is higher than

Table 2 Elemental composition of $NHPC_2$ determined by XPS and elemental analyses

Elemental analysis (wt%)			XPS (wt%)		
C	N	O	C	N	O
87.66	2.28	10.06	83.45	3.03	13.52

2%, and the oxygen content in $NHPC_2$ is about 10%. XPS measurement showed a similar result. The presence of nitrogen and oxygen could provide a hydrophilic and wettability characteristic for $NHPC_2$, demonstrating that $NHPC_2$ has a suitable heteroatom content, and a higher specific surface area with hierarchically porous structure at the same time.

High-resolution C 1s spectrum of $NHPC_2$ is presented in Fig. 5b. Several distinct peaks are found, including a main C–C peak at 284.6 eV, C–N peak centered at 285.3 eV, C–O peak at 286.6 eV, and C=O/C=N peaks at 289.1 eV [5, 13, 14]. As shown in Fig. 5c, high-resolution N 1s spectrum is adequately fitted by three component peaks, namely, pyridinic N (N-6, 398.6 eV), pyrrolic N (N-5, 400.5 eV), and quaternary N (N-Q, 401.3 eV), respectively [19, 42].

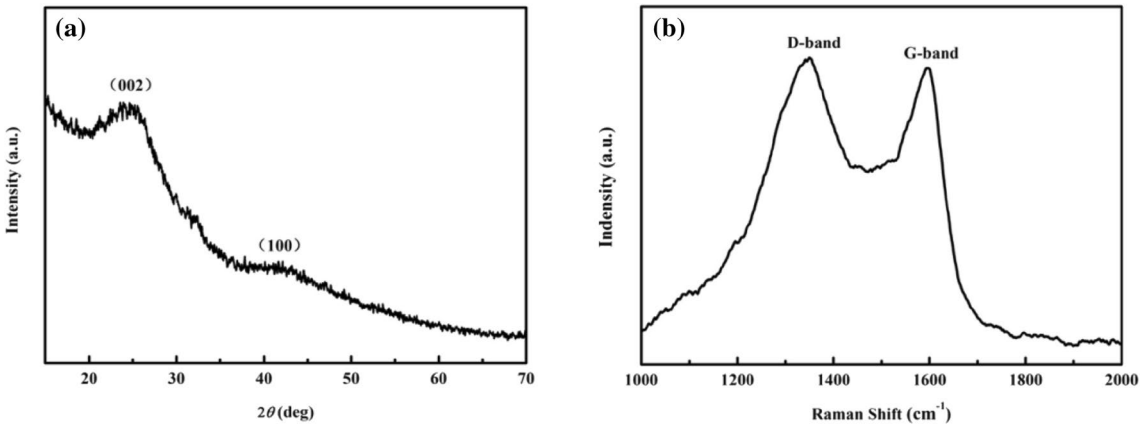

Fig. 4 **a** XRD pattern and **b** Raman spectrum of $NHPC_2$

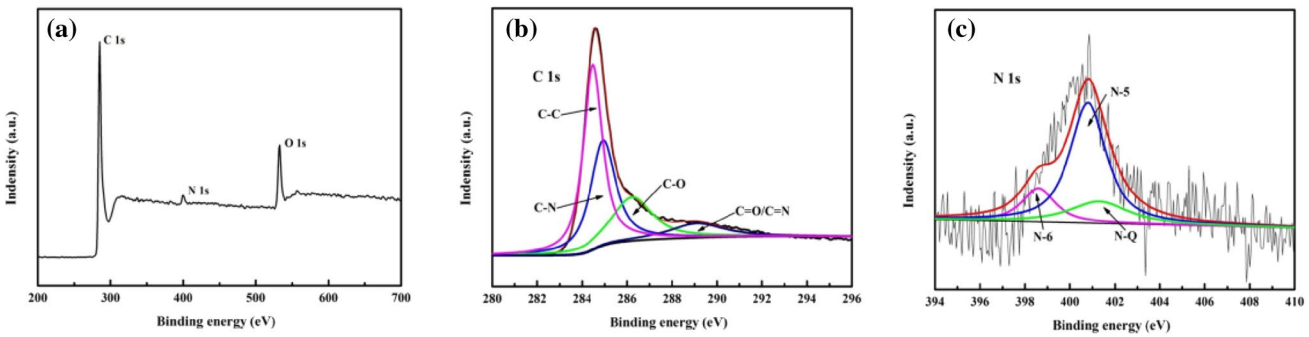

Fig. 5 **a** XPS survey spectrum, **b** high-resolution C 1s and **c** N 1s spectrum of $NHPC_2$

As known, the quaternary N bonded to three carbon atoms could enhance conductivity, and also, the presence of pyridinic N and pyrrolic N could induce pseudocapacitance for carbon materials [18]. Therefore, in our experiment, it is reasonable to consider that the nitrogen species (N-5, N-6, N-Q) in $NHPC_2$ contribute to the capacitance performance.

3.2 Electrochemical performance in the three-electrode system

Owing to the hierarchically porous structure and nitrogen-containing functional groups, $NHPC_2$ is expected to be a candidate high-performance electrode material for supercapacitors. The CV and GCD results for $NHPC_2$ at different scan rates and current densities are shown in Fig. 6. CV curves show a slightly distorted quasi-rectangular shape in Fig. 6a, suggesting the formation of an electrical double layer [29]. At a higher sweep rate of 100 mV s^{-1}, the quasi-rectangular shape is still well preserved, indicating an excellent capacitance behavior and fast diffusion of electrolyte ions into $NHPC_2$ [43].

Figure 6b depicts the GCD curves of $NHPC_2$ at different current densities. At the current density of 0.5 A g^{-1}, $NHPC_2$ exhibits a high specific capacitance of 287 F g^{-1}, which is 7.7% higher than that of chitin-derived heteroatom-doped porous carbon (266.5 F g^{-1}). The superior capacitance of $NHPC_2$ is possibly due to its higher BET specific surface area (chitin-derived carbon ~ 1745 m^2 g^{-1}), as the nitrogen contents of them are nearly the same [29]. The specific capacitances of $NHPC_2$ are as high as 273 and 242 F g^{-1} at 1 and 2 A g^{-1}, respectively, which are comparable or even higher than that of numerous porous carbon materials reported previously [44]. This good performance might be due to the synergistic effect of the large specific surface area, suitable pore size distribution and nitrogen doping. It should be emphasized that, even at a higher current density of 10 A g^{-1}, $NHPC_2$ still maintains a decent specific capacitance of 213 F g^{-1}, which is 74% of the initial capacitance at 0.5 A g^{-1}, indicating an excellent rate capability.

The cyclic stability of $NHPC_2$ was studied by GCD measurement at the current density of 5 A g^{-1}. Figure 6c exhibits a slight variation of specific capacitance with the increasing

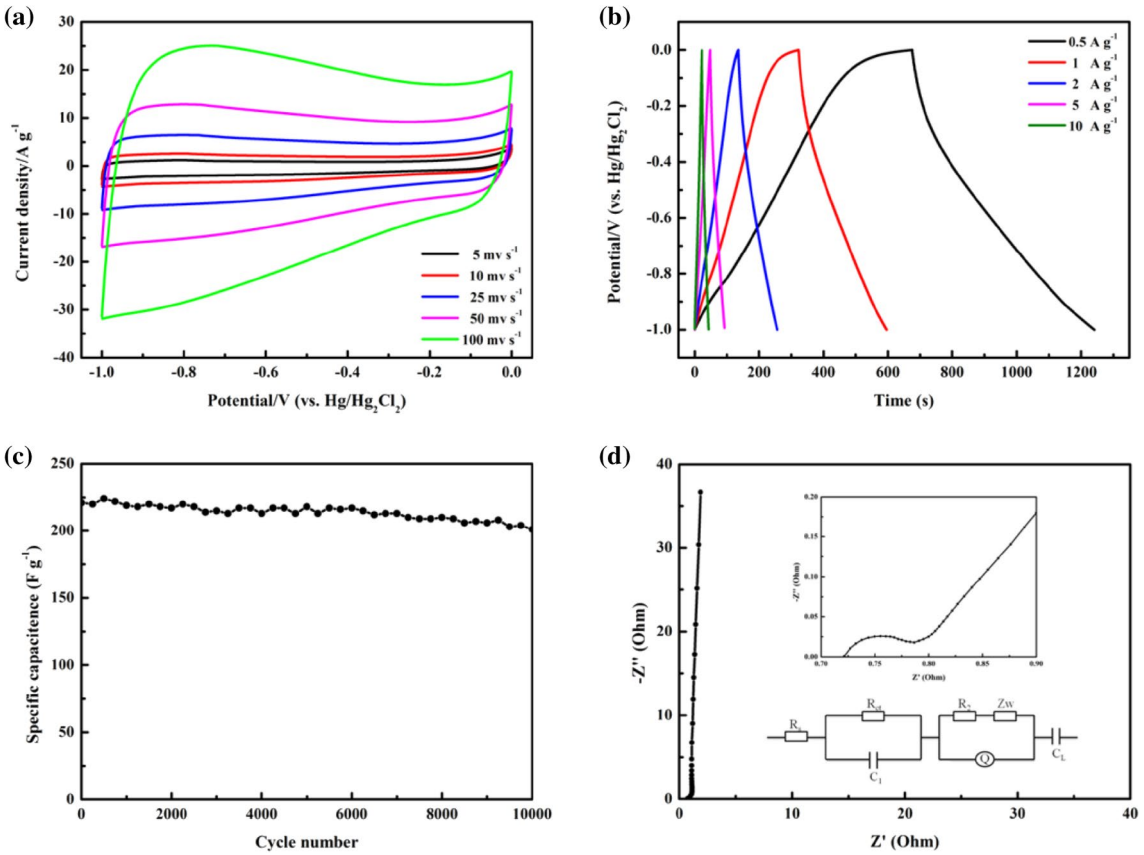

Fig. 6 **a** Electrochemical performances of $NHPC_2$. Representative cyclic voltammograms for the $NHPC_2$ electrode at different scan rates. **b** Charge–discharge curves at different constant current densities. **c** Cyclic stability of $NHPC_2$ electrode at the charge–discharge current density of 5 A g^{-1} for 10,000 cycles. **d** EIS results for $NHPC_2$ electrode in 6.0 M KOH, and the inset showed the magnified medium–high frequency region and the equivalent circuit

cycle numbers. After a long-term cyclic charge–discharge process (10,000 cycles), about 93% of the initial specific capacitance (221 F g^{-1}) is retained, which illustrates that $NHPC_2$ displays excellent cyclic stability. It is interesting to notice that the specific capacitance of $NHPC_2$ increases after a slight decrease during the long-term cyclic process. This might be owing to the effects from the doped nitrogen and oxygen or in situ activation of the electrode to expose additional surface area [18].

EIS measurement was employed to further investigate the resistive behavior of the $NHPC_2$ electrode for supercapacitors. The Nyquist plots are presented in Fig. 6d, and the equivalent circuit used to fit the impedance curves is shown in the inset of Fig. 6d. In terms of this EIS result, the Nyquist plot could be divided into three parts: a semicircle at high frequencies, a slash (about 45°) and a nearly vertical line at low frequencies. In the equivalent circuit, R_s represents the resistance related to the ionic conductivity of the electrolyte and the electronic conductivity of the electrodes and current collectors; R_{ct} is the charge-transfer resistance; C_1 is the capacitance of the electrode materials; R_2 is the interfacial resistance between the surface of electrode and electrolyte solution; Q is the constant phase element accounting for a double-layer capacitance at the interface; Zw is the Warburg resistance from the ion diffusion and transport in the electrolyte, and C_L is the limit capacitance [3, 6]. According to the fitted result, the R_s here is 0.72 Ω, indicating a pretty low equivalent series resistance. Charge transfer resistance (R_{ct}) of 0.05 Ω calculated from the radius of the semicircle in the high-frequency region confirms a quick charge transfer process, and the R_2 of 0.61 Ω implies an interfacial resistance which may be caused by the high content of oxygen. In the low-frequency region, the Nyquist plot is a straight line for an EDLC supercapacitor, which behaves as an ideal capacitor.

3.3 A comparison of $NHPC_2$ and fibroin-derived porous carbons

Silk cocoons consist of two components: fibroin, the key structural protein, and sericin, a waste protein that is abandoned during degumming process [20]. Actually, using cocoon or fibroin as precursor to develop supercapacitor electrode materials has recently been reported [15, 16, 19, 45]. In this experiment, the specific capacitances of sericin-derived $NHPC_2$ and fibroin-derived nitrogen-doped porous carbon (prepared via pre-carbonization and 1:2 KOH activation) were compared (Fig. 7). As shown, at the current densities ranging from 0.5 to 10 A g^{-1}, the specific capacitance of $NHPC_2$ is about 20 F g^{-1} higher than that of the fibroin-derived carbon. This might be because that the cylindrical appearance of fibroin hindered the sufficient

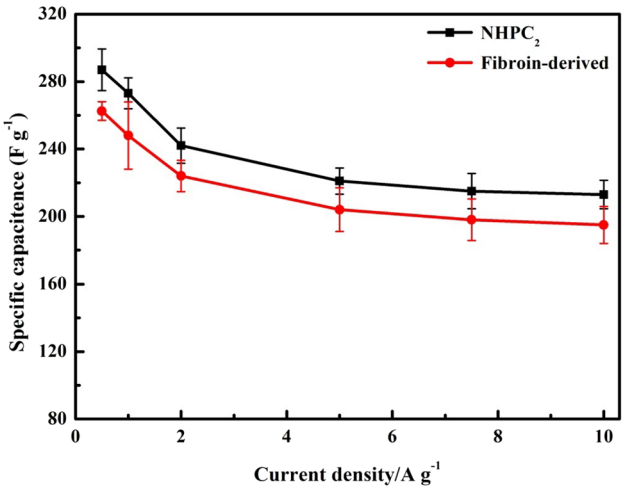

Fig. 7 A comparation of the specific capacitances between sericin and fibroin-derived porous carbons at various current densities

contact with KOH, resulting in a smaller specific surface area (Fig. S3). Nevertheless, the fibroin-derived porous carbon still shows an attractive electrochemical performance. At the current density of 10 A g^{-1}, it has a specific capacitance of 195 F g^{-1}, which is significantly higher than that of many cellulose-derived porous carbons [33, 44], suggesting that using protein as the raw material is an effective strategy to develop high-performance nitrogen-doped supercapacitor electrode materials.

3.4 Electrochemical performance in the two-electrode system

The excellent capacitive performances of $NHPC_2$-based electrodes were further tested in a two-electrode system. As shown in Fig. 8a, the $NHPC_2$-based symmetrical device displays characteristic capacitive behavior with quasi-rectangular-shaped CV curves even at a higher scan rate of 100 mV s^{-1}, demonstrating the charge transfer rate within $NHPC_2$ was rapid and effective. The GCD curves exhibits outstanding performance with a considerable specific capacitance of 183.2 F g^{-1} at the current density of 0.5 A g^{-1}, while maintaining a decent value of 144 F g^{-1} at a high current density of 10 A g^{-1} (Fig. 8b, c). From the Ragone plot for the $NHPC_2$-based electrode (Fig. 8d), it is observed that the energy density is 6.13 Wh kg^{-1} at the current density of 1 A g^{-1}. As the current density increases to 5 A g^{-1}, the energy density and power density are 5.35 Wh kg^{-1} and 2500.30 W kg^{-1}, respectively. It demonstrates that the $NHPC_2$-based electrode is very promising for the practical energy storage devices owing to the desirable electrochemical performance.

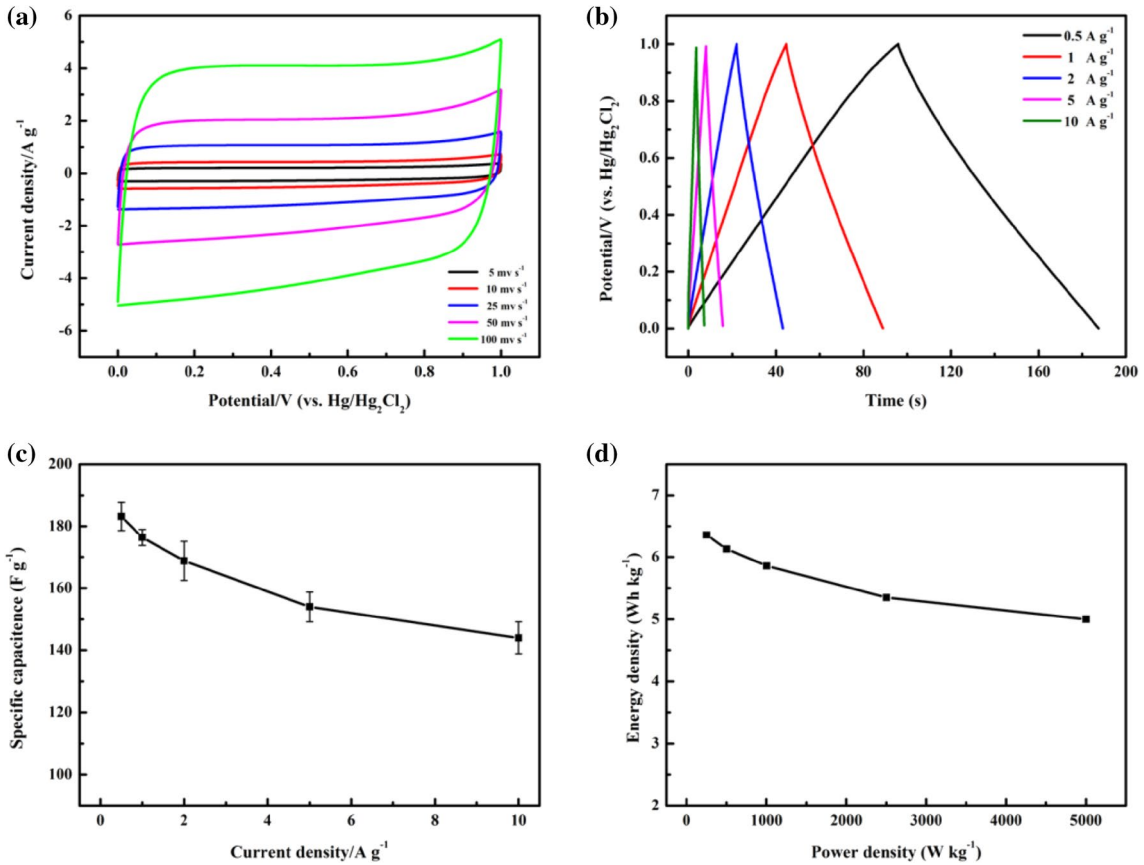

Fig. 8 Electrochemical performance characteristics of $NHPC_2$ tested in a two-electrode system. **a** CV curves at different scan rates. **b** GCD curves at different current densities. **c** The specific capacitances of single electrode at various current densities. **d** Ragone plot of $NHPC_2$, the power densities and energy densities from the charge–discharge curves at different current densities

4 Conclusions

In this work, nitrogen-doped hierarchically porous carbon has been successfully prepared from sericin using a two-step pre-carbonization and KOH activation method. The as-prepared $NHPC_2$ possesses a suitable nitrogen content and higher specific surface area with hierarchically porous structure. Benefited from the unique composition and microstructure, the $NHPC_2$ material demonstrated a high specific capacitance, superior rate capability, and excellent cycle stability. This work not only developed a high-performance supercapacitor electrode material from the waste sericin protein, but also provided a strategy for its disposal issue and contributed to the environmental improvement. Furthermore, the methodology established in this research is green, low-cost, and sustainable, and might shed light on the utilization of waste protein to prepare high-performance supercapacitor electrode materials.

Acknowledgements We are grateful for the financial support from Natural Science Foundation of Jiangsu province (Nos. BK20171295 and BK20150507), the China Postdoctoral Science Foundation (Nos. 2015M580392, 2015M580393), and the Jiangsu Province Postdoctoral Science Foundation (Nos. 1501025B, 1601231C).

References

1. C. Chen, D. Yu, G. Zhao, B. Du, W. Tang, L. Sun, Y. Sun, F. Besenbacher, M. Yu, Three-dimensional scaffolding framework of porous carbon nanosheets derived from plant wastes for high-performance supercapacitors. Nano Energy **27**, 377–389 (2016)
2. H. Wang, Z. Xu, A. Kohandehghan, Z. Li, K. Cui, X. Tan, T.J. Stephenson, C.K. Kingondu, C.M.B. Holt, B.C. Olsen, J.K. Tak, D. Harfield, A.O. Anyia, D. Mitlin, Interconnected carbon nanosheets derived from hemp for ultrafast supercapacitors with high energy. ACS Nano **7**, 5131–5141 (2013)
3. Y. Gong, D. Li, C. Luo, Q. Fu, C. Pan, Highly porous graphitic biomass carbon as advanced electrode materials for supercapacitors. Green Chem. **19**, 4132–4140 (2017)
4. Y. Huang, J. Tao, W. Meng, M. Zhu, Y. Huang, Y. Fu, Y. Gao, C. Zhi, Super-high rate stretchable polypyrrole-based supercapacitors with excellent cycling stability. Nano Energy **11**, 518–525 (2015)
5. L. Wan, E. Shamsaei, C.D. Easton, D. Yu, Y. Liang, X. Chen, Z. Abbasi, A. Akbari, X. Zhang, H. Wang, ZIF-8 derived nitrogen-doped porous carbon/carbon nanotube composite for high performance supercapacitor. Carbon **121**, 330–336 (2017)

6. Y. Ping, Y. Gong, Q. Fu, C. Pan, Preparation of three-dimensional graphene foam for high performance supercapacitors. Prog. Nat. Sci. **27**, 177–181 (2017)
7. J. Yang, H. Wu, M. Zhu, W. Ren, Y. Lin, H. Chen, F. Pan, Optimized mesopores enabling enhanced rate performance in novel ultrahigh surface area meso-/microporous carbon for supercapacitors. Nano Energy **33**, 453–461 (2017)
8. X. Chen, R. Paul, L. Dai, Carbon-based supercapacitors for efficient energy storage. Natl. Sci. Rev. **4**, 453–489 (2017)
9. Y. Yang, Y. Hao, J. Yuan, L. Niu, F. Xia, In situ preparation of caterpillar-like polyaniline/carbon nanotube hybrids with core shell structure for high performance supercapacitors. Carbon **78**, 279–287 (2014)
10. P. Xu, J. Kang, J. Choi, J. Suhr, J. Yu, F. Li, J. Byun, B. Kim, T. Chou, Laminated ultrathin chemical vapor deposition graphene films based stretchable and transparent high-rate supercapacitor. ACS Nano **8**, 9437–9445 (2014)
11. J. Cai, H. Niu, H. Wang, H. Shao, J. Fang, J. He, H. Xiong, C. Ma, T. Lin, High-performance supercapacitor electrode from cellulose-derived, inter-bonded carbon nanofibers. J. Power Sources **324**, 302–308 (2016)
12. J. Tang, R.R. Salunkhe, J. Liu, N.L. Torad, M. Imura, S. Furukawa, Y. Yamauchia, Thermal conversion of core–shell metal–organic frameworks: a new method for selectively functionalized nanoporous hybrid carbon. J. Am. Chem. Soc. **137**, 1572–1580 (2015)
13. Y. Zhao, C. Hu, Y. Hu, H. Cheng, G. Shi, L. Qu, A versatile, ultralight, nitrogen-doped graphene framework. Angew. Chem. Int. Ed. **51**, 11371–11375 (2012)
14. M. Lu, Y. Qian, C. Yang, X. Huang, H. Li, X. Xie, L. Huang, W. Huang, Nitrogen-enriched pseudographitic anode derived from silk cocoon with tunable flexibility for microbial fuel cells. Nano Energy **32**, 382–388 (2016)
15. Y. Yun, S. Cho, J. Shim, B. Kim, S. Chang, S. Baek, Y. Huh, Y. Tak, Y. Park, S. Park, H. Jin, Microporous carbon nanoplates from regenerated silk proteins for supercapacitors. Adv. Mater. **25**, 1993–1998 (2013)
16. V. Sahu, S. Grover, B. Tulachan, M. Sharma, G. Srivastava, M. Roy, M. Saxena, N. Sethy, K. Bhargava, D. Philip, H. Kim, G. Singh, S.K. Singh, M. Das, R.K. Sharma, Heavily nitrogen doped, graphene supercapacitor from silk cocoon. Electrochim. Acta **160**, 244–253 (2015)
17. Z. Li, Z. Xu, X. Tan, H. Wang, C.M.B. Holt, T. Stephenson, B.C. Olsenab, D. Mitlin, Mesoporous nitrogen-rich carbons derived from protein for ultra-high capacity battery anodes and supercapacitors. Energy Environ. Sci. **6**, 871–878 (2013)
18. W. Qian, F. Sun, Y. Xu, L. Qiu, C. Liu, S. Wang, F. Yan, Human hair-derived carbon flakes for electrochemical supercapacitors. Energy Environ. Sci. **7**, 379–386 (2014)
19. J. Hou, C. Cao, F. Idrees, X. Ma, Hierarchical porous nitrogen-doped carbon nanosheets derived from silk for ultrahigh-capacity battery anodes and supercapacitors. ACS Nano **9**, 2556–2564 (2015)
20. G. Wu, P. Song, D. Zhang, Z. Liu, L. Li, H. Huang, H. Zhao, N. Wang, Y. Zhu, Robust composite silk fibers pulled out of silkworms directly fed with nanoparticles. Int. J. Biol. Macromol. **104**, 533–538 (2017)
21. F. Wang, T. Cao, Y. Zhang, Effect of silk protein surfactant on silk degumming and its properties. Mater. Sci. Eng. C **55**, 131–136 (2015)
22. L. Lamboni, M. Gauthier, G. Yang, Q. Wang, Silk sericin: a versatile material for tissue engineering and drug delivery. Biotechnol. Adv. **33**, 1855–1867 (2015)
23. H. Yun, M.K. Kim, H.W. Kwak, J.Y. Lee, M.H. Kim, K.H. Lee, The role of glycerol and water in flexible silk sericin film. Int. J. Biol. Macromol. **82**, 945–951 (2016)
24. Y.N. Jo, I.C. Um, Effects of solvent on the solution properties, structural characteristics and properties of silk sericin. Int. J. Biol. Macromol. **78**, 287–295 (2015)
25. J. Li, W.L. Liu, D. Xiao, X.H. Wang, Oxygen-rich hierarchical porous carbon made from pomelo peel fiber as electrode material for supercapacitor. Appl. Surf. Sci. **416**, 918–924 (2017)
26. C. Liang, J.P. Bao, C.G. Li, H. Huang, C.L. Chen, Y. Lou, H.Y. Lu, H.B. Lin, Z. Shi, S.H. Feng, One-dimensional hierarchically porous carbon from biomass with high capacitance as supercapacitor materials. Microporous Mesoporous Mater. **251**, 77–82 (2017)
27. K. Wang, N. Zhao, S.W. Lei, R. Yan, X.D. Tian, J.Z. Wang, Y. Song, D.F. Xu, Q.G. Guo, L. Liu, Promising biomass-based activated carbons derived from willow catkins for high performance supercapacitors. Electrochim. Acta **166**, 1–11 (2017)
28. J. Sodtipinta, C. Ieosakulrat, N. Poonyayant, P. Kidkhunthod, N. Chanlek, T. Amornsakchai, P. Pakawatpanurut, Interconnected open-channel carbon nanosheets derived from pineapple leaf fiber as a sustainable active material for supercapacitors. Ind. Crops Prod. **104**, 13–20 (2017)
29. J. Zhou, L. Bao, S. Wu, W. Yang, H. Wang, Chitin based heteroatom-doped porous carbon as electrode materials for supercapacitors. Carbohyd. Polym. **173**, 321–329 (2017)
30. L. Zhang, Z. Liu, G. Cui, L. Chen, Biomass-derived materials for electrochemical energy storages. Prog. Polym. Sci. **43**, 136–164 (2015)
31. W.W. Kang, B.P. Lin, G.X. Huang, C.X. Zhang, Y.H. Yao, W.T. Hou, B. Xu, B.L. Xing, Peanut bran derived hierarchical porous carbon for supercapacitor. J. Mater. Sci.: Mater. Electron. **29**, 6361–6368 (2018)
32. H.W. Wang, C. Wang, Y. Xiong, C.D. Jin, Q.F. Sun, Simple synthesis of N-doped interconnected porous carbon from Chinese tofu for high-performance supercapacitor and lithium-ion battery applications. J. Electrochem. Soc **164**, A3832–A3839 (2017)
33. C. Wang, Y. Xiong, H.W. Wang, N. Yang, C.D. Jin, Q.F. Sun, "Pickles method" inspired tomato derived hierarchical porous carbon for high-performance and safer capacitive output. J. Electrochem. Soc **165**, A1054-A1063 (2018)
34. C. Wang, Y. Xiong, H.W. Wang, C.D. Jin, Q.F. Sun, Naturally tridimensional laminated porous carbon networks structured short nano-chains bridging nanospheres for energy storage. J. Mater. Chem. A **5**, 15759–15770 (2017)
35. Z.J. Wang, Y.Z. Lu, Y. Yan, T.Y.P. Larissa, X. Zhang, D. Wuu, H. Zhang, Y.H. Yang, X. Wang, Core-shell carbon materials derived from metalorganic frameworks as an efficient oxygen bifunctional electrocatalyst. Nano Energy **30**, 368–378 (2016)
36. T.L. Cai, H.W. Wang, C.D. Jin, Q.F. Sun, Y.J. Nie, Fabrication of nitrogen-doped porous electrically conductive carbon aerogel from waste cabbage for supercapacitors and oil/water separation. J. Mater. Sci.: Mater. Electron. **29**, 4334–4344 (2018)
37. T.T. Yang, Y.L. Xi, Y.K. Zhu, J.Z. Li, X.X. Pan, V.Y. Izotov, Q. Guo, W. Han, Black aspergillus-derived highly porous carbon fibers for capacitive applications. J. Mater. Sci.: Mater. Electron. **28**, 17592–17600 (2017)
38. Y. Lu, N.W. Zhu, F.H. Yin, T.T. Yang, P.X. Wu, Z. Dang, M.L. Liu, X.R. Wei, Biomass-derived heteroatoms-doped mesoporous carbon for efficient oxygen reduction in microbial fuel cells. Biosens. Bioelectron. **98**, 350–356 (2017)
39. P.W. Xiao, Q.H. Meng, L. Zhao, J.J. Li, Z.X. Wei, B.H. Han, Biomass-derived flexible porous carbon materials and their applications in supercapacitor and gas adsorption. Mater. Des. **129**, 164–172 (2017)
40. D.C. Qin, S. Chen, A sustainable synthesis of biomass carbon sheets as excellent performance sodium ion batteries anode. J. Solid State Electrochem. **21**, 1305–1312 (2017)

41. H.W. Wang, C.M. Sheng, T.L. Cai, C.D. Jin, Q.F. Sun, C. Wang, Mesopore-dominant nitrogen-doped carbon with a large defect degree and high conductivity via inherent hydroxyapatite-induced self-activation for lithium-ion batteries. RSC Adv. **8**, 12204–12210 (2018)
42. M. Zhou, F. Pu, Z. Wang, S.Y. Guan, Nitrogen-doped porous carbons through KOH activation with superior performance in supercapacitors. Carbon **68**, 185–194 (2014)
43. X.L. Su, M.Y. Cheng, L. Fu, J.H. Yang, X.C. Zheng, X.X. Guan, Superior supercapacitive performance of hollow activated carbon nanomesh with hierarchical structure derived from poplar catkins. J. Power Sources **362**, 27–38 (2017)
44. Z. Gao, Y. Zhang, N. Song, X. Li, Biomass-derived renewable carbon materials for electrochemical energy storage. Mater. Res. Lett. **5**, 69–88 (2017)
45. C. Long, Y. Xiao, M.T. Zheng, H. Hu, H.W. Dong, B.F. Lei, H.R. Zhang, J.L. Zhuang, Y.L. Liu, Nitrogen-doped porous carbon with an ultrahigh specific surface area for superior performance supercapacitors. J. Power Sources **310**, 145–153 (2016)